

Elastic scattering of the proton drip line nuclei ${}^7\text{Be}$, ${}^8\text{B}$, and ${}^9\text{C}$ on a lead target at energies around three times the Coulomb barriers

Y. Y. Yang,¹ X. Liu,¹ D. Y. Pang,^{2,3,*} D. Patel,¹ R. F. Chen,¹ J. S. Wang,^{1,†} P. Ma,¹ J. B. Ma,¹ S. L. Jin,¹ Z. Bai,¹ V. Guimarães,⁴ Q. Wang,¹ W. H. Ma,¹ F. F. Duan,¹ Z. H. Gao,¹ Y. C. Yu,¹ Z. Y. Sun,¹ Z. G. Hu,¹ S. W. Xu,¹ S. T. Wang,¹ D. Yan,¹ Y. Zhou,¹ Y. H. Zhang,¹ X. H. Zhou,¹ H. S. Xu,¹ G. Q. Xiao,¹ and W. L. Zhan¹

¹CAS Key Laboratory of High Precision Nuclear Spectroscopy, Institute of Modern Physics, Chinese Academy of Sciences, Lanzhou 730000, China

²School of Physics and Nuclear Energy Engineering, Beihang University, Beijing 100191, China

³International Research Center for Nuclei and Particles in the Cosmos, Beihang University, Beijing 100191, China

⁴Instituto de Física, Universidade de São Paulo, Rua do Matão, 1371, São Paulo 05508-090, SP, Brazil



(Received 15 November 2017; revised manuscript received 1 April 2018; published 15 October 2018)

Elastic scattering angular distributions of the proton drip line nucleus, ${}^9\text{C}$, impinging on a ${}^{\text{nat}}\text{Pb}$ target have been measured for the first time at energies around three times the Coulomb barriers at the Radioactive Ion Beam Line in Lanzhou. The same measurements were made for ${}^8\text{B}$ and ${}^7\text{Be}$ simultaneously. The measured elastic scattering angular distribution of ${}^9\text{C}$ on a lead target does not show any particular reduction at around the Coulomb rainbow angles, suggesting that the breakup coupling effect on the elastic scattering channel is very small in this energy region. A similar observation is made for ${}^8\text{B}$. Analysis with the continuum discretized coupled channels (CDCC) method shows that it is the Coulomb and/or the centrifugal barriers exerted on the valence protons that counteract the breakup coupling effects on the elastic scattering channel. CDCC calculations assuming ${}^9\text{C}$ to have a ${}^7\text{Be} + 2p$ cluster structure give elastic scattering cross sections similar to those for a ${}^8\text{B} + p$ structure. The calculated breakup cross sections with these two assumed structures of ${}^9\text{C}$ differ quite a bit at around the Coulomb rainbow angles, suggesting that the breakup cross sections, instead of the elastic scattering ones, are more sensitive to the structure of proton-rich nuclei at incident energies around three times the Coulomb barriers.

DOI: [10.1103/PhysRevC.98.044608](https://doi.org/10.1103/PhysRevC.98.044608)

I. INTRODUCTION

Halo nuclei have been one of the main interests of nuclear physicists over the last decades [1–12]. The proton drip line nucleus, ${}^9\text{C}$, with the low two-proton separation energy of 1.43 MeV, can be considered as a two-proton halo candidate. The ${}^9\text{C}$ nucleus plays a prominent role in the solar neutrino problem, e.g., in low-metallicity supermassive stars, and it takes part in the explosive hydrogen burning process (hot pp chain), which is expected to be a possible alternative path to the synthesis of CNO elements [13]. Special attention has recently been devoted to experimental and theoretical studies of the exotic nature of ${}^9\text{C}$ [14–18].

In 1997, Blank *et al.* measured the one-proton removal cross sections (σ_{1p}) for ${}^8\text{B}$ and ${}^9\text{C}$ and the two-proton removal cross section (σ_{2p}) for ${}^9\text{C}$ on targets varying from carbon to lead at the energy of 285 MeV per nucleon, based on the projectile-fragment separator of the GSI [14]. The measured σ_{2p} values are 2–3 times larger than those for σ_{1p} , depending slightly on the target nuclei, strongly suggesting a diproton configuration for ${}^9\text{C}$ (${}^9\text{C} \rightarrow {}^7\text{Be} + 2p$). Later, in 2003 and

2004, Enders *et al.* [15] and Warner *et al.* [16] measured σ_{1p} for ${}^8\text{B}$ and ${}^9\text{C}$ and σ_{2p} for ${}^9\text{C}$ on carbon and silicon targets at lower energies (76 and 78 MeV/nucleon and 20–70 MeV/nucleon, respectively), and the σ_{2p}/σ_{1p} ratio from both experiments was found to be systematically consistent with those obtained by Blank *et al.* [14]. Similarly, in the theoretical analyses of ${}^9\text{C}$ breakup within a three-body coupled channel framework, Fukui *et al.* found that the description of $p + {}^8\text{B}$ for ${}^9\text{C}$ is not sufficient and proposed that the extension of the calculation to incorporate the $p + p + {}^7\text{Be}$ configuration is important for a deeper understanding of the ${}^9\text{C}$ breakup [17]. Recently, Kobayashi *et al.* further proposed that the cluster breaking in the core (possibly $\alpha + {}^3\text{He}$ [18]) results in a significant enhancement of the diproton component in ${}^9\text{C}$, and this component markedly depends on the strength of the spin-orbit interaction since a diproton is fragile and dissociates readily due to the spin-orbit interaction [19]. The density distribution and root-mean-square radius of nuclear matter of ${}^9\text{C}$ have recently been extracted from the angular distribution of proton- ${}^9\text{C}$ elastic scattering at high energies (~ 300 MeV/nucleon) [20,21].

Elastic scattering induced by weakly bound nuclei is of paramount importance, as it contains information about the exotic structure and reaction mechanism of weakly bound nuclei [22]. Many experiments have been performed at

*dypang@buaa.edu.cn

†jswang@impcas.ac.cn

incident energies around the Coulomb barriers for the elastic scattering of neutron-halo nuclei, such as ${}^6\text{He}$ [5,23–29], ${}^{11}\text{Li}$ [30], and ${}^{11}\text{Be}$ [8,31–33]. Unlike well-bound nuclei, their elastic scattering angular distributions with respect to the Rutherford cross sections exhibit, near the Coulomb barrier, a Fresnel pattern [34] that is strongly suppressed or even disappears completely. The Fresnel pattern, also called the Coulomb rainbow, originates from the interference between the repulsive Coulomb and the attractive nucleon-nucleon potentials. Continuum discretized coupled channels (CDCC) calculations indicated that the suppression of Coulomb nuclear interference peaks (CNIPs) in the angular distributions of elastic scattering induced by neutron-rich nuclei is due to coupling effects on breakup channels [34]. The weakly bound nature of these nuclei causes them to be easily excited into continuum states during their collision with a target nucleus, igniting the breakup channels.

Our previous experimental results for ${}^8\text{B}$, which is an archetype of the proton halo nucleus, on a ${}^{\text{nat}}\text{Pb}$ target at 170.3 MeV show that, in spite of its low proton separation energy (0.136 MeV), there is no such strong breakup coupling effect in its angular distributions [35]. This fact, in contrast to the cases of neutron-rich nuclei, has been studied systematically by comparing the elastic scattering angular distributions of ${}^8\text{B}$ and the neutron-rich nucleus ${}^{11}\text{Be}$ with both medium-mass and heavy targets at incident energies from the vicinity of the Coulomb barrier to about three times the Coulomb barrier using the CDCC method. It was found that the difference in the elastic scattering cross sections in ${}^8\text{B}$ vs ${}^{11}\text{Be}$ can be attributed to the Coulomb and centrifugal barriers encountered by the valence proton in the ground state of ${}^8\text{B}$ [36], which suppressed the breakup coupling effects.

The breakup coupling effects on the elastic scattering cross sections of ${}^9\text{C}$ are not clear yet, owing to the lack of experimental data. In this paper, we present the results of our new experimental data on ${}^9\text{C}$ elastic scattering from a ${}^{\text{nat}}\text{Pb}$ target at energies above the Coulomb barriers. The same measurement for ${}^7\text{Be}$ and ${}^8\text{B}$ has also been made. Due to the limitation of our detector systems, we were not able to separate the elastic scattering events from the inelastic ones. The experimental data reported in this paper are on quasielastic scattering. However, within the angular range covered by our measurement, the contributions from the inelastic channels are negligible. Because of this, we can treat our data as elastic scattering data. Breakup coupling effects on the elastic scattering channel for ${}^9\text{C}$ and ${}^8\text{B}$ are investigated using the CDCC method.

II. EXPERIMENT AND DATA ANALYSES

The experiment was performed at the National Laboratory of Heavy Ion Research of the Institute of Modern Physics. The secondary beams of radioactive isotopes were produced by the fragmentation of the ${}^{12}\text{C}^{6+}$ primary beam on a ${}^9\text{Be}$ target with a thickness of 2652 μm using the Heavy Ion Research Facility of Lanzhou (HIRFL) [37,38]. The secondary beams, ${}^7\text{Be}$, ${}^8\text{B}$, and ${}^9\text{C}$, were separated by their magnetic rigidity and delivered by the Radioactive Ion Beam Line in Lanzhou (RIBLL) [39,40] and impinged on a ${}^{\text{nat}}\text{Pb}$ target.

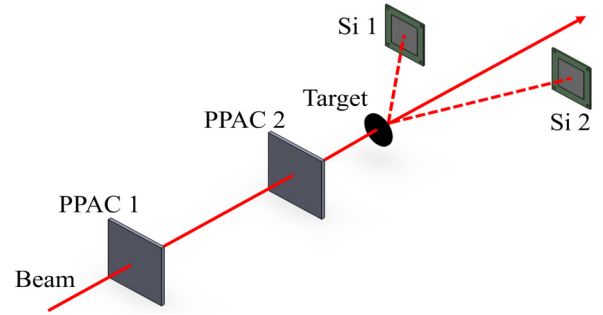


FIG. 1. Sketch of the experimental setup for our measurements.

The ${}^{\text{nat}}\text{Pb}$ target was a self-supporting foil with a thickness of 4.2 mg/cm^2 and had the following isotopic composition: ${}^{208}\text{Pb}$ (52.3%), ${}^{207}\text{Pb}$ (22.6%), ${}^{206}\text{Pb}$ (23.6%), and ${}^{204}\text{Pb}$ (1.48%). It is usually believed that low incident energies are preferred in studying the nuclear structure and reaction mechanisms in elastic scattering measurements. However, being produced in a projectile-fragmentation-type facility, the secondary proton-rich particles have relatively high energies, around 30 MeV/nucleon. These particles were slowed down with aluminum degraders to about 20 MeV/nucleon. A further decrease in the beam energy will result in an unacceptable beam intensity. For these practical reasons, the energies of the secondary beams in the laboratory system were about three times the corresponding Coulomb barriers at the center of the targets, namely, 130 MeV for ${}^7\text{Be}$, 178 MeV for ${}^8\text{B}$, and 227 MeV for ${}^9\text{C}$. A sketch of the experimental setup is shown in Fig. 1. A 301- μm -thick aluminum plate, located on the second focal plane (F2) of the RIBLL, was utilized to degrade the incident energy and to improve the purity of the secondary beams. The beam intensities of ${}^7\text{Be}$, ${}^8\text{B}$, and ${}^9\text{C}$ were 1.5×10^4 pps (particles per second), 1×10^3 pps, and 5×10^2 pps, respectively. Secondary beams were identified using a time-of-flight and energy loss (ToF- ΔE) technique with a certain magnetic rigidity. The ToF was measured with two 50- μm -thick plastic scintillators located on the second (F2) and fourth (F4) focal planes of the RIBLL. The energy loss for each beam was measured with a 280- μm -thick silicon detector at F4. During the experiment, the ΔE detector was removed from the beam line to avoid the disturbance in the beams since the ToF itself was enough to identify the particles in the cocktail beam.

Two position-sensitive parallel-plate avalanche counters (PPACs), with a position resolution of 1 mm, were fixed in front of the ${}^{\text{nat}}\text{Pb}$ target, at distances of 100 and 500 mm, respectively. Each PPAC had 80 gold-plated tungsten wires as anode in both the X and the Y directions. The tungsten wires, 20 μm in diameter, were spaced 1 mm apart, providing a sensitive area of $80 \times 80 \text{ cm}^2$. The signals from the strip electrodes were connected to a delay line with a 4-ns delay between neighboring wires. The actual position and direction of the beam on the target were obtained by connecting the two hit points on the PPACs and extending to the target plane event by event.

Elastic scattering events were detected using two sets of ΔE - E silicon telescopes, which consisted of a double-sided

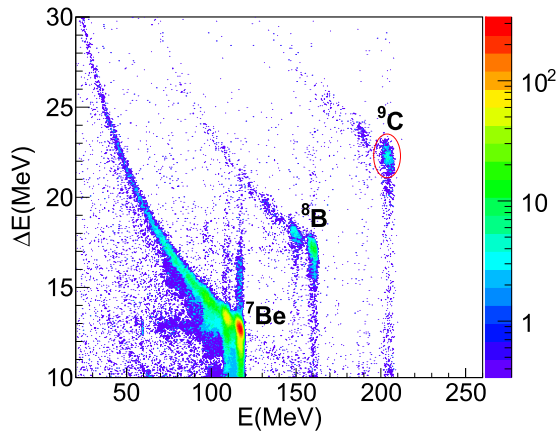


FIG. 2. Two-dimensional spectra for ${}^9\text{C}$, ${}^8\text{B}$, and ${}^7\text{Be}$ projectile nuclei. Points on the solid red ellipsoid curve represent events in the elastic scattering of ${}^9\text{C}$.

silicon strip detector (48 strips of 1-mm width, each including a 0.1-mm interval) with a thickness of $150\ \mu\text{m}$ and a large surface silicon detector with a thickness of $1500\ \mu\text{m}$. Each telescope covered a polar angle of 7° – 30° in the laboratory frame, on either side of the beam axis. The distances from the ${}^{\text{nat}}\text{Pb}$ target to the center of the telescopes were 247 and 201 mm, respectively. A typical two-dimensional spectra, for ${}^9\text{C}$, ${}^8\text{B}$, and ${}^7\text{Be}$, is shown in Fig. 2. It can be clearly seen that all three proton drip line nuclei are well separated. The corresponding band for each nucleus shows three peaks. Two of them are identified to originate from single and double sequential hits on tungsten wires of the PPACs. Elastic scattering events have been identified by applying an energy window to each spectrum in the off-line data analysis. Details of our experimental setup and procedures of data analysis can be found in Ref. [41].

Elastic scattering angles have been determined using the incident position and direction of the beam on the target provided by PPACs and the hitting point on the Si telescopes. In order to consider the broad and nonuniform beam profiles on the target, a Monte Carlo simulation has also been performed to evaluate the absolute differential cross sections. More detailed descriptions of the adopted procedure for data normalization and detector misalignment correction are given in Refs. [35,41,42]. The above-mentioned simulation allowed for the elimination of any systematic error arising from the target thickness, total number of incoming beam particles, and solid angles.

III. RESULTS AND DISCUSSION

Our results on quasielastic scattering angular distributions, normalized to the Rutherford cross sections, for ${}^9\text{C}$, ${}^8\text{B}$, and ${}^7\text{Be}$ with a ${}^{\text{nat}}\text{Pb}$ target are shown in Fig. 3. The error bars in Fig. 3 are for statistical errors only. It was difficult to separate elastic events from inelastic ones due to the 1.7% energy dispersion of our secondary beam and the limited energy resolution of our silicon detectors, which was around 0.8%. Since ${}^9\text{C}$ and ${}^8\text{B}$ have no bound excited states, the inelastic channels are mainly collective excitations of the target nucleus. As

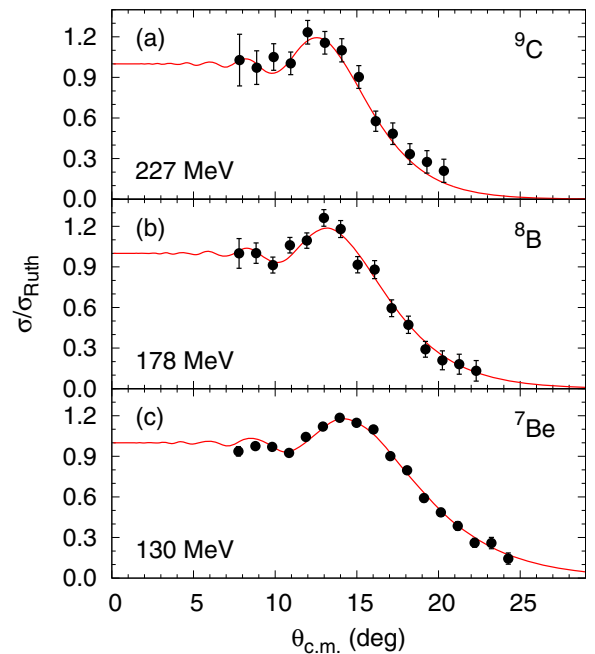


FIG. 3. Experimentally measured elastic scattering angular distributions for (a) ${}^9\text{C}$, (b) ${}^8\text{B}$, and (c) ${}^7\text{Be}$ on a ${}^{\text{nat}}\text{Pb}$ target at 227, 178, and 130 MeV, respectively. Solid curves represent results of optical model calculations with the systematic nucleus-nucleus potential by Xu and Pang [44]. See details in the text.

we have discussed in Refs. [41] and [42], the contributions of target excitations to our experimental data are negligible within the angular range covered in our measurements. One distinct feature of these data is that their angular distributions are of the Fresnel diffraction pattern, which is typical for well-bound nucleus-nucleus scattering [43]. There is no Coulomb rainbow suppression as seen in cases of neutron-rich nuclei at energies around the Coulomb barriers, which is known to be caused by the breakup coupling effect [34]. One may argue that the incident energy in our experiment is too high for the breakup coupling effects to manifest in the elastic angular distributions. Our systematic calculations with the CDCC method for ${}^8\text{B}$ and ${}^{11}\text{Be}$ on medium-mass and heavy targets, however, show that the incident energy does not play a dominant role in these cases [36]. The CNIP in the elastic scattering of ${}^{11}\text{Be}$ is strongly suppressed even at relatively high energies, around three times the Coulomb barriers. In order to examine our predictions made in Ref. [36], we have recently made a measurement of ${}^{11}\text{Be}$ elastic scattering from a lead target at 141 MeV. The data are being analyzed and the results will be published in the near-future.

We first analyze our data with optical model calculations. These are made with the systematic nucleus-nucleus potential of Xu and Pang [44], which is based on a single-folding model [45,46] using the Bruyères Jeukenne-Lejeune-Mahaux semimicroscopic nucleon-nucleus potential [47,48]. This potential can reasonably account for the elastic scattering and the total reaction cross sections for projectiles with $A \gtrsim 6$ on heavy targets with $A \gtrsim 40$ for incident energies from near the Coulomb barrier to around 100 MeV/nucleon [44]. The

proton and neutron density distributions for the nuclei were taken from Hartree-Fock calculations with the SkX interaction [49]. The root-mean-square radii of these proton distributions are 2.371 fm (2.36 ± 0.02 fm [50]), 2.537 fm (2.49 ± 0.03 fm [51]), 2.628 fm, and 5.441 fm (5.442 ± 0.02 fm [52]) for ${}^7\text{Be}$, ${}^8\text{B}$, ${}^9\text{C}$, and ${}^{208}\text{Pb}$, respectively. Values in parentheses are the corresponding experimental ones. As shown in Fig. 3, results of these optical model calculations reproduce the experimental data quite well within the error bars.

The corresponding total reaction cross sections of these optical model calculations are $\sigma_{\text{total}} = 3063, 3263,$ and 3396 mb for ${}^7\text{Be}$, ${}^8\text{B}$, and ${}^9\text{C}$, at incident energy $E_{\text{lab}} = 130, 178,$ and 227 MeV, respectively. These total reaction cross sections and their error bars are determined by both the uncertainties in the systematic optical potentials, which are about 15% in the renormalization factors of the real and imaginary parts (Nr and Ni, respectively; see Ref. [44]), and the experimental error bars in the elastic scattering cross sections. We run series of optical model calculations with Nr and Ni changed by factors of from 0.85 to 1.15, in steps of 0.05. χ^2 values are found for each run with respect to the experimental data. The mean values and standard deviations of the total reaction cross section, which are those reported at the beginning of this paragraph, are then found by averaging the resulting total reaction cross sections of these optical model calculations weighted by their corresponding $1/\chi^2$ values. These total reaction cross sections can be compared with each other and with the other systems by considering the scaling procedure proposed in Ref. [53], with which the cross sections and the incident energies are divided by the factors $(A_p^{1/3} + A_t^{1/3})^2$ and $Z_p Z_t e^2 / (A_p^{1/3} + A_t^{1/3})$, respectively. This procedure would scale the normal geometrical and/or charge differences between systems without washing out the dynamical effects of interest. The resulting reduced total cross sections for ${}^7\text{Be}$, ${}^8\text{B}$, and ${}^9\text{C}$ are $\sigma_{\text{reduced}} = \sigma_{\text{total}} / (A_p^{1/3} + A_t^{1/3})^2 = 49.8, 51.9,$ and 52.9 mb, respectively, which are consistent with the asymptotic value of 50.0 mb for weakly bound and exotic nuclei [54].

The fact that our data can be reproduced rather well with optical model calculations, which do not treat the breakup channels explicitly, using systematic potentials which were obtained from elastic scattering data on stable nuclei suggests that the breakup coupling effects on the elastic scattering cross sections are very small for these proton-rich nuclei at about three times the Coulomb barrier energies. In order to study the breakup coupling effects explicitly, we have performed CDCC calculations for ${}^9\text{C}$ and ${}^8\text{B}$ with the computer code FRESKO [55]. Test calculations have been performed with the mass numbers of the lead targets ranging from $A = 204$ to $A = 208$. Differences in the resulting elastic scattering cross sections with these mass numbers are negligible, therefore, a mass number $A = 208$ of the target is considered in the following analysis.

First, we model the ${}^9\text{C}$ nucleus as a diproton plus an inert ${}^7\text{Be}$ core (${}^9\text{C} \rightarrow {}^7\text{Be} + 2p$). For simplicity, both the valence protons are assumed to be in the $0p_{3/2}$ orbital with their spins coupled to 0 and their center-of-mass orbits the ${}^7\text{Be}$ core with zero angular momentum. The binding potential of the

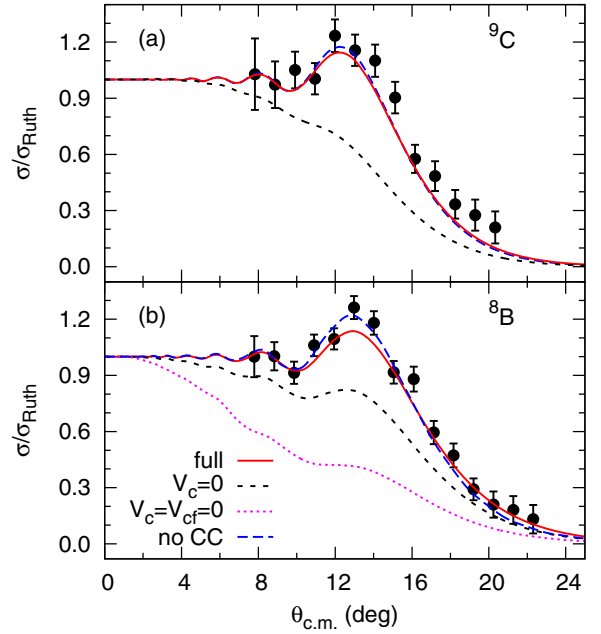


FIG. 4. Elastic scattering cross sections from CDCC calculations for (a) ${}^9\text{C} + {}^{208}\text{Pb}$ at 227 MeV and (b) ${}^8\text{B} + {}^{208}\text{Pb}$ at 178 MeV, together with the experimental values. Solid, short-dashed, and dotted curves represent results of the full calculations, of the calculations without Coulomb forces in the core-valence interaction ($V_c = 0$), and of the calculations without Coulomb and centrifugal barriers in ($V_c = V_{cf} = 0$), respectively. Dashed curves show results calculated without couplings to continuum states (no CC).

$2p$ - ${}^7\text{Be}$ system was taken to be of Woods-Saxon form with a reduced radius $r_0 = 1.25$ fm and a diffuseness parameter $a_0 = 0.65$ fm. The depth of this binding potential was adjusted to reproduce the two-proton separation energy in the ground state of ${}^9\text{C}$, which is 1.436(2) MeV [56]. The same potential is used for the continuum states of the $2p$ - ${}^7\text{Be}$ system. The $2p$ - ${}^7\text{Be}$ relative orbital angular momenta up to $\ell_{\text{max}} = 3$ were included with all couplings up to a maximum multipolarity $\lambda_{\text{max}} = 3$. The continuum states up to a maximum $2p$ - ${}^7\text{Be}$ relative energy of $\varepsilon_{\text{max}} = 26.90$ MeV, which corresponds to a maximum momentum $k_{\text{max}} = 0.9$ fm $^{-1}$, were discretized into eight equally spaced bins of width $\Delta k = 0.1$ fm $^{-1}$, giving a total of 36 bins. The systematic single-folding potential described above has been used for the ${}^7\text{Be} + {}^{208}\text{Pb}$ optical potential at 176.6 MeV. The depth of the $2p + {}^{208}\text{Pb}$ potential at 50.4 MeV was taken to be twice that of the $p + {}^{208}\text{Pb}$ potential evaluated at 25.2 MeV with the KD02 systematics [57]. For comparisons, calculations not taking into account the continuum couplings were also made. Similar calculations were performed for ${}^8\text{B}$ (${}^8\text{B} \rightarrow {}^7\text{Be} + p$). The results are shown in Fig. 4. One sees that the results taking and not taking into account the continuum couplings, as shown by the solid and dashed curves, respectively, are very close to each other and they both reproduce the experimental data reasonably well for both the ${}^9\text{C} + {}^{208}\text{Pb}$ and the ${}^8\text{B} + {}^{208}\text{Pb}$ systems. The CDCC calculations underestimate the ${}^9\text{C}$ data at larger angles. It will be interesting to see if full four-body CDCC calculations can improve the description of these data

at these angles. In a study of elastic scattering of ${}^6\text{He}$ with a dineutron model, Moro *et al.* found that by changing the binding energy of the dineutron in the ground state of ${}^6\text{He}$ from its experimental value (0.97 MeV) to 1.6 MeV, the dineutron wave function could mimic some properties of the three-body wave function of ${}^6\text{He}$. This change in the dineutron binding energy also helped to reproduce the elastic scattering of ${}^6\text{He}$ from various target nuclei at incident energies around the Coulomb barriers [58]. However, we have not followed this procedure in this work. In fact, we have shown that the diproton model with an experimental binding energy reproduced the elastic scattering data on ${}^9\text{C}$ with a lead target quite well at energies well above the Coulomb barrier. This fact itself is rather interesting. Further study is highly desirable to determine whether it is due to the higher incident beam energy required for the structure of ${}^9\text{C}$ to show up in its elastic scattering angular distribution or to the two charged valence nucleons of ${}^9\text{C}$, which cause reactions induced by ${}^9\text{C}$ to be different from those induced by neutron-rich nuclei such as ${}^6\text{He}$. A four-body CDCC calculation for ${}^9\text{C}$ is expected to answer these questions.

In Ref. [36] we have attributed the persistence of the CNIP in the elastic scattering cross sections of ${}^8\text{B}$ on a ${}^{208}\text{Pb}$ target to the Coulomb and centrifugal barriers between the core nucleus and the valence proton. When these barriers are removed in CDCC calculations, the CNIP in the elastic scattering cross sections of ${}^8\text{B}$ is greatly reduced, resembling those that have been observed with neutron-rich nuclei such as ${}^{11}\text{Be}$ [34]. The same analysis is made of the results of our new measurement presented in this paper. The results are shown in Figs. 4(a) and 4(b) for ${}^9\text{C}$ and ${}^8\text{B}$, respectively; the short-dashed and the dotted curves are elastic scattering cross sections calculated without the Coulomb and the centrifugal barriers in the valence-core systems, respectively, within the CDCC framework. The nuclear potentials are refitted to reproduce the experimental binding energy of the valence protons in the ground states of ${}^9\text{C}$ and ${}^8\text{B}$. Again, one observes, as in Ref. [36], that the CNIPs are greatly reduced when these barriers are removed in CDCC calculations.

CDCC calculations assuming that ${}^9\text{C}$ is composed of a valence proton (in the $0p_{3/2}$ orbital) and a ${}^8\text{B}$ core are also performed. The result is shown as the dashed blue curve in Fig. 5. The previous result assuming a diproton structure (${}^7\text{Be} + 2p$) of ${}^9\text{C}$ is shown as the solid red curve for comparisons. It is interesting to see that the two results are close to each other and both reproduced the experimental results within the error bars, although the calculated cross section assuming a ${}^8\text{B} + p$ configuration is slightly larger than that for a ${}^7\text{Be} + 2p$ one. This similarity between the results from the CDCC calculations with the two assumed configurations of ${}^9\text{C}$ (${}^8\text{B} + p$ and ${}^7\text{Be} + 2p$) may be understood from the fact that the ${}^7\text{Be} + 2p$ system has a higher Coulomb barrier than the ${}^8\text{B} + p$ system does, which, to some extent, compensates the lack of centrifugal barrier in the former compared to the latter. In both cases, the existence of Coulomb and centrifugal barriers suppressed the breakup channels from having strong coupling effects on the elastic scattering channel and allowed the CNIPs to persist in the elastic scattering of proton-rich nuclei with heavy targets even for

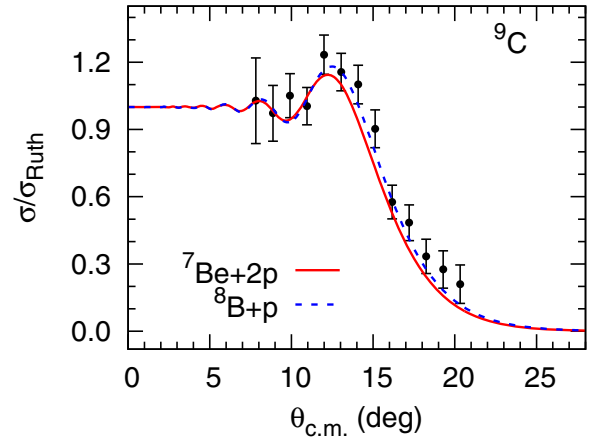


FIG. 5. Results of CDCC calculations for the elastic scattering angular distributions of ${}^9\text{C}$ on ${}^{208}\text{Pb}$ at 227 MeV with the two assumed structures of ${}^9\text{C}$, ${}^7\text{Be} + 2p$ (solid red curve) and ${}^8\text{B} + p$ (dashed blue curve), and comparisons with the experimental data. See the text for details.

projectiles like ${}^8\text{B}$, which has a very low single-particle binding energy.

Results of the analysis above suggest that elastic scattering with heavy targets (such as ${}^{208}\text{Pb}$) at relatively high incident energies (at three times the Coulomb barriers, for instance) is not very sensitive to the structure of proton-rich nuclei. The breakup cross sections, on the other hand, are more sensitive to the structure of proton-rich nuclei. We demonstrate this point in Fig. 6, where results of CDCC calculations are shown for the breakup cross sections of ${}^9\text{C}$ with a ${}^{208}\text{Pb}$ target at 227 MeV, assuming it to have a ${}^8\text{B} + p$ and a ${}^7\text{Be} + 2p$ cluster structure, respectively. The corresponding elastic scattering cross sections are shown as well. All these cross sections are normalized to the Rutherford cross sections. One sees that,

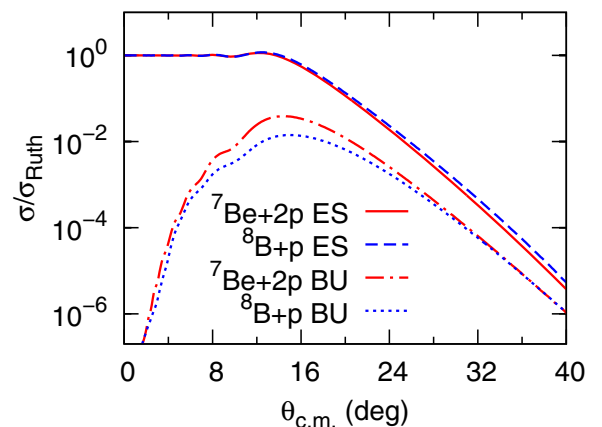


FIG. 6. Results of CDCC calculations for the elastic scattering (ES) and breakup (BU) cross sections as functions of the scattering angles for ${}^9\text{C}$ on a ${}^{208}\text{Pb}$ target at 227 MeV. Solid and dashed red curves represent elastic scattering, and dash-dotted and dotted blue curves show breakup cross sections, for the two assumed structures of ${}^9\text{C}$: ${}^8\text{B} + p$ and ${}^7\text{Be} + 2p$, respectively. All these results are presented as ratios to the Rutherford cross sections.

within all scattering angles plotted, the elastic scattering cross sections are almost the same for the two assumed cluster configurations of ${}^9\text{C}$. However, the breakup cross section assuming a ${}^7\text{Be} + 2p$ structure of the ground state of ${}^9\text{C}$ is about 2.5 times larger than that obtained assuming a ${}^8\text{B} + p$ structure at around 14° in the center-of-mass system, which is also at the angle of the CNIP in the elastic scattering cross sections.

IV. SUMMARY

In summary, results on elastic scattering of ${}^9\text{C}$ from a ${}^{\text{nat}}\text{Pb}$ target at 227 MeV are presented in this paper, which was measured for the first time at the RIBLL facility. Results of the same measurement made for ${}^8\text{B}$ and ${}^7\text{Be}$ at 178 and 130 MeV, respectively, are also shown. The angular distributions of the elastic scattering induced by these light proton-drip nuclei possess Coulomb nuclear interference peaks, which are typical in the elastic scattering of well-bound nuclei. These data can be reasonably well reproduced by CDCC and optical model calculations using the systematic nucleus-nucleus potential of Ref. [44], which was obtained by analyzing experimental data on stable nuclei. Analysis with CDCC calculations suggests that it is the Coulomb and

centrifugal barriers in the valence-core systems that prevent the breakup channels from coupling strongly to the elastic scattering channel. Our results show that elastic scattering measured with heavy targets at incident energies as high as around three times the Coulomb barriers is not sensitive to the single-particle structure of light proton-rich nuclei. A comparison of the elastic scattering and breakup cross sections calculated for ${}^9\text{C}$ assuming a $2p + {}^7\text{Be}$ and a $p + {}^8\text{B}$ structure suggests that breakup cross sections are sensitive to the structure.

ACKNOWLEDGMENTS

We are grateful to the staff members of the HIRFL for the operation of the cyclotron and those of the RIBLL for their friendly collaboration. This work was financially supported by the National Natural Science Foundation of China (Grants No. U1432247, No. 11575256, No. 11775013, No. U1632138, and No. 11705242), the National Key R&D Program of China (Contract No. 2018YFA0404403), and the National Key Research and Development Program (Grant No. 2016YFA0400502). This work was also supported by the CAS Light of West China Program under Grant No. Y601030XB0.

-
- [1] I. Tanihata, H. Hamagaki, O. Hashimoto, Y. Shida, N. Yoshikawa, K. Sugimoto, O. Yamakawa, T. Kobayashi, and N. Takahashi, *Phys. Rev. Lett.* **55**, 2676 (1985).
- [2] T. Aumann, D. Aleksandrov, L. Axelsson, T. Baumann, M. J. G. Borge, L. V. Chulkov, J. Cub, W. Dostal, B. Eberlein, T. W. Elze, H. Emling, H. Geissel, V. Z. Goldberg, M. Golovkov, A. Grünschoß, M. Hellström, K. Hencken, J. Holeczek, R. Holzmann, B. Jonson, A. A. Korshennikov, J. V. Kratz, G. Kraus, R. Kulesa, Y. Leifels, A. Leistenschneider, T. Leth, I. Mukha, G. Münzenberg, F. Nickel, T. Nilsson, G. Nyman, B. Petersen, M. Pfützner, A. Richter, K. Riisager, C. Scheidenberger, G. Schrieder, W. Schwab, H. Simon, M. H. Smedberg, M. Steiner, J. Stroth, A. Surowiec, T. Suzuki, O. Tengblad, and M. V. Zhukov, *Phys. Rev. C* **59**, 1252 (1999).
- [3] V. Lapoux, N. Alamanos, F. Auger, Y. Blumenfeld, J.-M. Casandjian, M. Chartier, M. Cortina-Gil, V. Fékou-Youmbi, A. Gillibert, J. Kelley, K. Kemper, M. M. Cormick, F. Maréchal, F. Marie, W. Mittig, F. de Oliveira Santos, N. Orr, A. Ostrowski, S. Ottini-Hustache, P. Roussel-Chomaz, J.-A. Scarpaci, J.-L. Sida, T. Suomijärvi, and J. Winfield, *Phys. Lett. B* **517**, 18 (2001).
- [4] N. Keeley, R. Raabe, N. Alamanos, and J. Sida, *Prog. Part. Nucl. Phys.* **59**, 579 (2007).
- [5] E. Benjamim, A. Lépine-Szily, D. M. Junior, R. Lichtenthäler, V. Guimarães, P. Gomes, L. Chamon, M. Hussein, A. Moro, A. Arazi, I. Padron, J. A. Nuñez, M. Assunção, A. Barioni, O. Camargo, R. Denke, P. de Faria, and K. Pires, *Phys. Lett. B* **647**, 30 (2007).
- [6] E. F. Aguilera, E. Martínez-Quiroz, D. Lizcano, A. Gómez-Camacho, J. J. Kolata, L. O. Lamm, V. Guimarães, R. Lichtenthäler, O. Camargo, F. D. Becchetti, H. Jiang, P. A. DeYoung, P. J. Mears, and T. L. Belyaeva, *Phys. Rev. C* **79**, 021601 (2009).
- [7] Y. Kucuk, I. Boztosun, and T. Topel, *Phys. Rev. C* **80**, 054602 (2009).
- [8] A. Di Pietro, G. Randisi, V. Scuderi, L. Acosta, F. Amorini, M. J. G. Borge, P. Figuera, M. Fisichella, L. M. Fraile, J. Gomez-Camacho, H. Jeppesen, M. Lattuada, I. Martel, M. Milin, A. Musumarra, M. Papa, M. G. Pellegriti, F. Perez-Bernal, R. Raabe, F. Rizzo, D. Santonocito, G. Scalia, O. Tengblad, D. Torresi, A. M. Vidal, D. Voulot, F. Wenander, and M. Zadro, *Phys. Rev. Lett.* **105**, 022701 (2010).
- [9] Y. Kucuk, *Nucl. Phys. A* **927**, 195 (2014).
- [10] R. Kumar and A. Bonaccorso, *Phys. Rev. C* **84**, 014613 (2011).
- [11] Y. Kucuk and A. M. Moro, *Phys. Rev. C* **86**, 034601 (2012).
- [12] A. Bonaccorso, D. M. Brink, and C. A. Bertulani, *Phys. Rev. C* **69**, 024615 (2004).
- [13] M. Wiescher, J. Görres, S. Graff, L. Buchmann, and F.-K. Thielemann, *Astrophys. J.* **343**, 352 (1989).
- [14] B. Blank, C. Marchand, M. Pravikoff, T. Baumann, F. Boué, H. Geissel, M. Hellström, N. Iwasa, W. Schwab, K. Sümmerer, and M. Gai, *Nucl. Phys. A* **624**, 242 (1997).
- [15] J. Enders, T. Baumann, B. A. Brown, N. H. Frank, P. G. Hansen, P. R. Heckman, B. M. Sherrill, A. Stolz, M. Thoennessen, J. A. Tostevin, E. J. Tryggstad, S. Typel, and M. S. Wallace, *Phys. Rev. C* **67**, 064301 (2003).
- [16] R. E. Warner, F. D. Becchetti, J. A. Brown, A. Galonsky, J. H. Kelley, A. Nadasen, R. M. Ronningen, J. A. Tostevin, J. S. Winfield, and P. Zecher, *Phys. Rev. C* **69**, 024612 (2004).
- [17] T. Fukui, K. Ogata, K. Minomo, and M. Yahiro, *Phys. Rev. C* **86**, 022801 (2012).
- [18] N. Furutachi, M. Kimura, A. Doté, and Y. Kanada-En'yo, *Prog. Theor. Phys.* **122**, 865 (2009).
- [19] F. Kobayashi and Y. Kanada-En'yo, *Phys. Rev. C* **89**, 024315 (2014).
- [20] Y. Matsuda, H. Sakaguchi, H. Takeda, S. Terashima, J. Zenihiro, T. Kobayashi, T. Murakami, Y. Iwao, T. Ichihara, T. Suda, T.

- Ohnishi, Y. Watanabe, H. Otsu, K. Yoneda, Y. Satou, K. Ozeki, and M. Kanazawa, *Phys. Rev. C* **87**, 034614 (2013).
- [21] S. Rafi, A. Bhagwat, W. Haider, and Y. K. Gambhir, *Phys. Rev. C* **89**, 067601 (2014).
- [22] J. J. Kolata, V. Guimarães, and E. F. Aguilera, *Eur. Phys. J. A* **52**, 123 (2016).
- [23] R. E. Warner, F. D. Becchetti, J. W. Jänecke, D. A. Roberts, D. Butts, C. L. Carpenter, J. M. Fetter, A. Muthukrishnan, J. J. Kolata, K. Lamkin, M. Belbot, M. Zahar, A. Galonsky, K. Ieki, and P. Zecher, *Phys. Rev. C* **51**, 178 (1995).
- [24] G. Ter-Akopian, A. Rodin, A. Fomichev, S. Sidorchuk, S. Stepantsov, R. Wolski, M. Chelnokov, V. Gorshkov, A. Lavrentev, V. Zagrebaev, and Y. Oganessian, *Phys. Lett. B* **426**, 251 (1998).
- [25] A. Di Pietro, P. Figuera, F. Amorini, C. Angulo, G. Cardella, S. Cherubini, T. Davinson, D. Leanza, J. Lu, H. Mahmud, M. Milin, A. Musumarra, A. Ninane, M. Papa, M. G. Pellegriti, R. Raabe, F. Rizzo, C. Ruiz, A. C. Shotter, N. Soić, S. Tudischo, and L. Weissman, *Phys. Rev. C* **69**, 044613 (2004).
- [26] L. Acosta, A. M. Sánchez-Benítez, M. E. Gómez, I. Martel, F. Pérez-Bernal, F. Pizarro, J. Rodríguez-Quintero, K. Rusek, M. A. G. Alvarez, M. V. Andrés, J. M. Espino, J. P. Fernández-García, J. Gómez-Camacho, A. M. Moro, C. Angulo, J. Cabrera, E. Casarejos, P. Demaret, M. J. G. Borge, D. Escrig, O. Tengblad, S. Cherubini, P. Figuera, M. Gulino, M. Freer, C. Metelko, V. Ziman, R. Raabe, I. Mukha, D. Smirnov, O. R. Kakuee, and J. Rahighi, *Phys. Rev. C* **84**, 044604 (2011).
- [27] O. Kakuee, M. Alvarez, M. Andrés, S. Cherubini, T. Davinson, A. D. Pietro, W. Galster, J. Gómez-Camacho, A. Laird, M. Laméhi-Rachti, I. Martel, A. Moro, J. Rahighi, A. Sánchez-Benítez, A. Shotter, W. Smith, J. Vervier, and P. Woods, *Nucl. Phys. A* **765**, 294 (2006).
- [28] K. Rusek, N. Keeley, K. W. Kemper, and R. Raabe, *Phys. Rev. C* **67**, 041604 (2003).
- [29] O. Kakuee, J. Rahighi, A. Sánchez-Benítez, M. Andrés, S. Cherubini, T. Davinson, W. Galster, J. Gómez-Camacho, A. Laird, M. Laméhi-Rachti, I. Martel, A. Shotter, W. Smith, J. Vervier, and P. Woods, *Nucl. Phys. A* **728**, 339 (2003).
- [30] M. Cubero, J. P. Fernández-García, M. Rodríguez-Gallardo, L. Acosta, M. Alcorta, M. A. G. Alvarez, M. J. G. Borge, L. Buchmann, C. A. Diget, H. A. Falou, B. R. Fulton, H. O. U. Fynbo, D. Galaviz, J. Gómez-Camacho, R. Kanungo, J. A. Lay, M. Madurga, I. Martel, A. M. Moro, I. Mukha, T. Nilsson, A. M. Sánchez-Benítez, A. Shotter, O. Tengblad, and P. Walden, *Phys. Rev. Lett.* **109**, 262701 (2012).
- [31] V. Pseudo, M. J. G. Borge, A. M. Moro, J. A. Lay, E. Nácher, J. Gómez-Camacho, O. Tengblad, L. Acosta, M. Alcorta, M. A. G. Alvarez, C. Andreoiu, P. C. Bender, R. Braid, M. Cubero, A. Di Pietro, J. P. Fernández-García, P. Figuera, M. Fisichella, B. R. Fulton, A. B. Garnsworthy, G. Hackman, U. Hager, O. S. Kirsebom, K. Kuhn, M. Lattuada, G. Marquínez-Durán, I. Martel, D. Miller, M. Moukaddam, P. D. O'Malley, A. Perea, M. M. Rajabali, A. M. Sánchez-Benítez, F. Sarazin, V. Scuderi, C. E. Svensson, C. Unsworth, and Z. M. Wang, *Phys. Rev. Lett.* **118**, 152502 (2017).
- [32] A. Di Pietro, V. Scuderi, A. M. Moro, L. Acosta, F. Amorini, M. J. G. Borge, P. Figuera, M. Fisichella, L. M. Fraile, J. Gomez-Camacho, H. Jeppesen, M. Lattuada, I. Martel, M. Milin, A. Musumarra, M. Papa, M. G. Pellegriti, F. Perez-Bernal, R. Raabe, G. Randisi, F. Rizzo, G. Scalia, O. Tengblad, D. Torresi, A. M. Vidal, D. Voulot, F. Wenander, and M. Zadro, *Phys. Rev. C* **85**, 054607 (2012).
- [33] M. Mazzocco, C. Signorini, M. Romoli, A. De Francesco, M. Di Pietro, E. Vardaci, K. Yoshida, A. Yoshida, R. Bonetti, A. De Rosa, T. Glodariu, A. Guglielmetti, G. Inglima, M. La Commara, B. Martin, D. Pierroutsakou, M. Sandoli, F. Soramel, L. Stroe, R. Kanungo, N. Khai, T. Motobayashi, T. Nomura, T. Ishikawa, H. Ishiyama, S. Jeong, H. Miyatake, M. H. Tanaka, I. Sugai, and Y. Watanabe, *Eur. Phys. J. A Hadrons Nuclei* **28**, 295 (2006).
- [34] N. Keeley, K. W. Kemper, and K. Rusek, *Eur. Phys. J. A* **50**, 145 (2014).
- [35] Y. Y. Yang, J. S. Wang, Q. Wang, D. Pang, J. B. Ma, M. R. Huang, J. L. Han, P. Ma, S. L. Jin, Z. Bai, Q. Hu, L. Jin, J. B. Chen, N. Keeley, K. Rusek, R. Wada, S. Mukherjee, Z. Y. Sun, R. F. Chen, X. Y. Zhang, Z. G. Hu, X. H. Yuan, X. G. Cao, Z. G. Xu, S. W. Xu, C. Zhen, Z. Q. Chen, Z. Chen, S. Z. Chen, C. M. Du, L. M. Duan, F. Fu, B. X. Gou, J. Hu, J. J. He, X. G. Lei, S. L. Li, Y. Li, Q. Y. Lin, L. X. Liu, F. D. Shi, S. W. Tang, G. Xu, X. Xu, L. Y. Zhang, X. H. Zhang, W. Zhang, M. H. Zhao, Z. Y. Guo, Y. H. Zhang, H. S. Xu, and G. Q. Xiao, *Phys. Rev. C* **87**, 044613 (2013).
- [36] Y. Y. Yang, X. Liu, and D. Y. Pang, *Phys. Rev. C* **94**, 034614 (2016).
- [37] J. Xia, W. Zhan, B. Wei, Y. Yuan, M. Song, W. Zhang, X. Yang, P. Yuan, D. Gao, H. Zhao, X. Yang, G. Xiao, K. Man, J. Dang, X. Cai, Y. Wang, J. Tang, W. Qiao, Y. Rao, Y. He, L. Mao, and Z. Zhou, *Nucl. Instrum. Methods Phys. Res. Sec. A: Accelerat. Spectrom. Detect. Assoc. Equip.* **488**, 11 (2002).
- [38] W. Zhan, J. Xia, H. Zhao, G. Xiao, Y. Yuan, H. Xu, K. Man, P. Yuan, D. Gao, X. Yang, M. Song, X. Cai, X. Yang, Z. Sun, W. Huang, Z. Gan, and B. Wei, *Nucl. Phys. A* **805**, 533c (2008).
- [39] W. Zhan, Z. Guo, G. Liu, J. Dang, R. He, S. Zhou, Q. Yin, Y. Luo, Y. Wang, B. Wei, Z. Sun, G. Xiao, J. Wang, S. Jiang, J. Li, X. Meng, W. Zhang, L. Qing, and Q. Wang, *Sci. China Ser. A: Math.* **42**, 528 (1999).
- [40] Z. Sun, W.-L. Zhan, Z.-Y. Guo, G. Xiao, and J.-X. Li, *Nucl. Instrum. Methods Phys. Res. Sec. A: Accelerat. Spectrom. Detect. Assoc. Equip.* **503**, 496 (2003).
- [41] Y. Y. Yang, J. S. Wang, Q. Wang, D. Y. Pang, J. B. Ma, M. R. Huang, P. Ma, S. L. Jin, J. L. Han, Z. Bai, L. Jin, J. B. Chen, Q. Hu, R. Wada, S. Mukherjee, Z. Y. Sun, R. F. Chen, X. Y. Zhang, Z. G. Hu, X. H. Yuan, S. W. Xu, S. Z. Chen, X. G. Lei, L. X. Liu, W. H. Ma, S. T. Wang, D. Yan, X. H. Zhang, M. H. Zhao, Y. Zhou, Y. J. Zhou, Z. Y. Guo, Y. H. Zhang, H. S. Xu, and G. Q. Xiao, *Phys. Rev. C* **90**, 014606 (2014).
- [42] Y. Yang, J. Wang, Q. Wang, J. Ma, M. Huang, J. Han, P. Ma, S. Jin, Z. Bai, Q. Hu, L. Jin, J. Chen, R. Wada, Z. Sun, R. Chen, X. Zhang, Z. Hu, X. Yuan, X. Cao, Z. Xu, S. Xu, C. Zhen, Z. Chen, Z. Chen, S. Chen, C. Du, L. Duan, F. Fu, B. Gou, J. Hu, J. He, X. Lei, S. Li, Y. Li, Q. Lin, L. Liu, F. Shi, S. Tang, G. Xu, X. Xu, L. Zhang, X. Zhang, W. Zhang, M. Zhao, Y. Zhang, and H. Xu, *Nucl. Instrum. Methods Phys. Res. Sec. A: Accelerat. Spectrom. Detect. Associat. Equip.* **701**, 1 (2013).
- [43] W. E. Frahn, *Ann. Phys.* **72**, 524 (1972).
- [44] Y. P. Xu and D. Y. Pang, *Phys. Rev. C* **87**, 044605 (2013).
- [45] D. Y. Pang, Y. L. Ye, and F. R. Xu, *Phys. Rev. C* **83**, 064619 (2011).

- [46] D. Y. Pang, Y. L. Ye, and F. R. Xu, *J. Phys. G: Nucl. Part. Phys.* **39**, 095101 (2012).
- [47] E. Bauge, J. P. Delaroche, and M. Girod, *Phys. Rev. C* **58**, 1118 (1998).
- [48] E. Bauge, J. P. Delaroche, and M. Girod, *Phys. Rev. C* **63**, 024607 (2001).
- [49] B. A. Brown, *Phys. Rev. C* **58**, 220 (1998).
- [50] I. Tanihata, T. Kobayashi, O. Yamakawa, S. Shimoura, K. Ekuni, K. Sugimoto, N. Takahashi, T. Shimoda, and H. Sato, *Phys. Lett. B* **206**, 592 (1988).
- [51] M. Obuti, T. Kobayashi, D. Hirata, Y. Ogawa, A. Ozawa, K. Sugimoto, I. Tanihata, D. Olson, W. Christie, and H. Wieman, *Nucl. Phys. A* **609**, 74 (1996).
- [52] J. Zenihiro, H. Sakaguchi, T. Murakami, M. Yosoi, Y. Yasuda, S. Terashima, Y. Iwao, H. Takeda, M. Itoh, H. P. Yoshida, and M. Uchida, *Phys. Rev. C* **82**, 044611 (2010).
- [53] P. R. S. Gomes, J. Lubian, I. Padron, and R. M. Anjos, *Phys. Rev. C* **71**, 017601 (2005).
- [54] J. J. Kolata and E. F. Aguilera, *Phys. Rev. C* **79**, 027603 (2009).
- [55] I. J. Thompson, *Comput. Phys. Rep.* **7**, 167 (1988).
- [56] M. Wang, G. Audi, A. Wapstra, F. Kondev, M. MacCormick, X. Xu, and B. Pfeiffer, *Chin. Phys. C* **36**, 1603 (2012).
- [57] A. J. Koning and J. P. Delaroche, *Nucl. Phys. A* **713**, 231 (2003).
- [58] A. M. Moro, K. Rusek, J. M. Arias, J. Gómez-Camacho, and M. Rodríguez-Gallardo, *Phys. Rev. C* **75**, 064607 (2007).